

OPEN ACCESS

The effects of retardation on plasmon hybridization within metallic nanostructures

To cite this article: Mark D Turner *et al* 2010 *New J. Phys.* **12** 083062

View the [article online](#) for updates and enhancements.

You may also like

- [Microscopic-Stress-Induced retardation between amorphous silicon nitride and amorphous indium zinc oxide having different stresses](#)
Nakcho Choi, Taekyung Yim, Yeogeon Yoon *et al.*
- [Residual stresses at cavity corners in silicon-on-insulator bonded wafers](#)
T-W Lin, O Elkhatib, J Makinen *et al.*
- [Simultaneous measurement of phase retardation and fast axis azimuth of wave plate based on equivalent component and phase detection](#)
Qianghua Chen, Jinhong Ding, Yu Guan *et al.*

The effects of retardation on plasmon hybridization within metallic nanostructures

Mark D Turner^{1,2}, Md Muntasir Hossain¹ and Min Gu^{1,3}

¹ Centre for Micro-Photonics and Centre for Ultrahigh-Bandwidth Devices for Optical Systems (CUDOS), Faculty of Engineering and Industrial Sciences, Swinburne University of Technology, VIC 3122, Australia

² CRC for Polymers, 8 Redwood Drive, Notting Hill, VIC 3168, Australia

E-mail: mgu@swin.edu.au

New Journal of Physics **12** (2010) 083062 (16pp)

Received 14 May 2010

Published 31 August 2010

Online at <http://www.njp.org/>

doi:10.1088/1367-2630/12/8/083062

Abstract. Plasmon hybridization theory (PHT) is an analytical model developed for understanding plasmonic interactions within complex metallic nanostructures, and gives a useful insight for optimizing design parameters. However, this theory is based on the electrostatic limit, which restricts the model to nanostructures much smaller than the free space wavelength of light. Here, we extend the PHT to incorporate retardation of the Coulomb interaction and investigate the effects of retardation on plasmons within metallic structures. We compare these results using other methods, such as Mie scattering theory and the finite integration technique, and observe a good agreement in both electrostatic and retardation regimes. Plasmons within metallic nanospheres and nanotubes are shown to have significant retardation in certain regimes, causing red-shifting to plasmon wavelengths, and we discuss the implications of retardation for plasmonic devices.

³ Author to whom any correspondence should be addressed.

Contents

1. Introduction	2
2. Retarded plasmon hybridization theory (RPHT)	3
3. Nanosphere	4
3.1. Derivation of retarded plasmon frequencies	4
3.2. Comparison of retarded plasmon hybridization theory (RPHT) and Mie theory	5
4. Nanotube	7
4.1. Stationary retarded plasmons	7
4.2. Propagating retarded plasmons	9
5. Conclusion	10
Acknowledgments	11
Appendix A. Iterative method for RPHT	11
Appendix B. Stationary nanotube plasmons	12
Appendix C. Propagating nanotube plasmons	14
References	15

1. Introduction

Metallic nanostructures (MNs) have recently received much interest for their unique plasmonic properties, useful for developing novel photonic devices. Through the design of the structure, metallic surfaces and metallic nanoparticles have the ability to be tailored for applications such as plasmonic solar cells [1]–[3], surface-enhanced Raman scattering [4]–[6], optical switching [7], high-resolution microscopy [8] and metamaterials [9]–[11].

Modeling plasmons and understanding the light–matter interaction within MNs are both essential for the design of useful photonic devices. The size (d) of a plasmonic nanoparticle is typically much smaller than the wavelength of operation, i.e. $\lambda \gg d$ [12]–[15]. Thus, the plasmonic system can be modeled under the much simpler electrostatic limit, that is typically valid for $d < \lambda/10$. For MNs with dimensions $d > \lambda/10$, which here we call the retardation regime, the electrostatic approximation is no longer valid and these methods based on the electrostatic limit produce significant errors [16].

Solving Maxwell’s equations analytically, semi-analytically or numerically using methods such as the Mie scattering theory [16], the multipole method [17], the finite-difference method [18] and the boundary element method [18] are commonly used in both electrostatic and retarded regimes. These methods are useful for simulating light propagation within these MNs and to model their optical properties. However, they do not give a complete physical understanding of the interactions between plasmons and their influences on the optical properties of MNs.

Plasmon hybridization theory (PHT) is an analytical model for calculating localized plasmon modes within complex MNs [12, 13, 19, 20]. As opposed to solving Maxwell’s equations, PHT is an analytical method that models the plasmon modes as oscillating fluids of electrons bound to the structure of the MN. This alternative method allows one to obtain a more intuitive understanding of the mechanisms that affect the dynamics of plasmons within these MNs. This can be helpful for designing MNs with specific optical properties, especially

when multiple metallic or dielectric surfaces are present. PHT has been developed in the electrostatic limit and thus ignores retardation effects on the Coulomb potential. For structures with $d > \lambda/10$, retardation effects become significant and plasmon frequencies are red-shifted, as investigated in [16] where plasmons within spherical nanoshells were modeled via Mie scattering theory.

Semi-analytical methods such as that developed in [14] can also be used to calculate plasmon modes in complex MNs, and this one was further developed to calculate the coupling between plasmons within a complex system [15]. However, methods such as PHT are developed within the electrostatic limit.

This paper has the following structure. In section 2, we extend electrostatic PHT to develop a retarded plasmon hybridization theory (RPHT) by including retardation effects into the Coulomb potential. In section 3, we use the RPHT to derive plasmon frequencies in metallic nanospheres and results are compared with Mie theory. We then consider a more complex MN in section 4 where the RPHT is used to model plasmons within metallic nanotubes with dielectric cores. In these results we observe both plasmon hybridization and retardation and provide a comparison with numerical solutions to validate these observed phenomena. Retardation is also shown to affect the dispersion of propagating plasmons within large-sized metallic nanotubes.

2. Retarded plasmon hybridization theory (RPHT)

Electrostatic PHT assumes that an MN consists of a uniform stationary positive background and a fluid of conduction electrons whose motion gives rise to plasmon oscillations [13]. The fluid is assumed to be of uniform density n_0 , incompressible, irrotational and no damping is present. These assumptions lead to relations for the MN plasmon frequencies in terms of the bulk metal Drude frequency $\omega_B^2 = 4\pi e^2 n_0 / m_e$, where e and m_e are the charge and mass of an electron, respectively [13].

Solutions to the fluid flow potential, $\eta(\mathbf{r})$ can be solved via Laplace's equation, $\nabla^2 \eta = 0$. The modal solutions to Laplace's equations form the basis set of the plasmon modes. Calculating the kinetic energy and electrical potential energy of this dynamic system leads to the plasmon eigenmodes of the MN and their corresponding modal frequencies. The kinetic energy (T) of the plasmon fluid is given by

$$T = \frac{n_0 m_e}{2} \oint \eta \vec{\nabla} \eta \cdot \hat{\mathbf{n}} dS, \quad (1)$$

where S is the surface of the MN with normal unit vector $\hat{\mathbf{n}}$. This term in the Lagrangian is not affected by retardation effects. The potential energy V of the system is given by

$$V = \frac{1}{2} \int \sigma(\mathbf{r}, t) \Phi(\mathbf{r}, t) dS, \quad (2)$$

where $\Phi(\mathbf{r}, t)$ is the retarded Coulomb potential and $\sigma(\mathbf{r}, t)$ is the surface charge distribution of the plasmon, which are given by

$$\sigma(\mathbf{r}, t) = n_0 e \int \vec{\nabla} \eta|_{\text{surface}} \cdot \hat{\mathbf{n}} dt \quad (3)$$

and

$$\Phi(\mathbf{r}, t) = \int \frac{\sigma(\mathbf{r}', t - |\mathbf{r} - \mathbf{r}'|/c)}{|\mathbf{r} - \mathbf{r}'|} dS', \quad (4)$$

where c is the speed of light in free space. The retarded Coulomb potential given by (4) is the integral of the retarded charge distribution over the surface S' of the MN. By using this definition of the Coulomb potential we consider retardation effects on plasmons within MNs. The addition of the temporal delay $t_d = |\mathbf{r} - \mathbf{r}'|/c$, causes a spatial–temporal coupling. However, if we assume that the solutions to the Lagrangian for the retarded system has the same form as that in the electrostatic case, i.e. a harmonic oscillator of frequency ω , then the spatial and temporal terms can be separated as

$$\sigma(\mathbf{r}, t - |\mathbf{r} - \mathbf{r}'|/c) = \sigma(\mathbf{r}, t) \cos\left(\frac{\omega}{c} |\mathbf{r} - \mathbf{r}'|\right). \quad (5)$$

In the electrostatic limit $\omega|\mathbf{r} - \mathbf{r}'|/c = 2\pi d/\lambda \ll 1$ and thus $\sigma(\mathbf{r}, t - |\mathbf{r} - \mathbf{r}'|/c) \approx \sigma(\mathbf{r}, t)$. However, when the size of the particle becomes significant, retardation will no longer be negligible. The effect of this term on (2) is to decrease the Coulomb potential energy and as we shall see later cause a red-shift to plasmon resonances. The Coulomb potential energy of the system then becomes

$$V = \frac{1}{2} \int \sigma(\mathbf{r}, t) \int \frac{\sigma(\mathbf{r}', t)}{|\mathbf{r} - \mathbf{r}'|} \cos\left(\frac{\omega}{c} |\mathbf{r} - \mathbf{r}'|\right) dS' dS. \quad (6)$$

We shall now use this RPHT to investigate plasmon modes within MNs for a metallic nanosphere in section 3 and a metallic nanotube in section 4.

3. Nanosphere

3.1. Derivation of retarded plasmon frequencies

In this section, we derive an expression for the plasmon frequencies of a metallic nanosphere with radius α , suspended in air using the RPHT. Spherical solutions of Laplace's equations are given by the set of orthonormal spherical harmonics,

$$\eta(r, \theta, \phi, t) = \sum_{l,m} a_{l,m}(t) r^l Y_{l,m}(\theta, \phi), \quad (7)$$

where $Y_{l,m}$ is the normalized real spherical harmonic function and $a_{l,m}(t)$ is the time-oscillating amplitude of the l, m mode. The kinetic energy $T_{l,m}$ of the l, m plasmon mode is given by [13]

$$T_{l,m} = \frac{n_o m_e}{2} l \alpha_{l,m}^2(t) \alpha^{2l+1}. \quad (8)$$

To solve for the Coulomb potential we shall use the spherical Green's function expansion given by [21]

$$\frac{1}{|\mathbf{r} - \mathbf{r}'|} = \sum_{i,j} \frac{4\pi}{\alpha(2l+1)} Y_{i,j}(\theta, \phi) Y_{i,j}(\theta', \phi'). \quad (9)$$

In general, when calculating the potential energy $V_{l,m}$ of the l, m plasmon mode, one should consider the coupling between different (p, q) plasmon modes:

$$V_{l,m} = \sum_{p,q} \frac{1}{2} \int \sigma(\mathbf{r}, t)_{l,m} \Phi_{p,q}(\mathbf{r}, t) dS. \quad (10)$$

These cross-coupling terms where $p, q \neq l, m$ are zero in the electrostatic regime due to orthogonality. However, they become non-zero in the retarded regime due to the introduction

of the retardation, which breaks the orthogonality condition. However, here we shall proceed and ignore these much smaller cross-coupling terms. Using (7) in (3), (6), (9) and (10) gives the potential energy $V_{l,m}$ for the l, m mode as

$$V_{l,m} = 2\pi n_o^2 e^2 \frac{l^2}{(2l+1)} \alpha^{2l+1} A_{l,m}^2(t) \sum_{i,j} N_{lmij}, \quad (11)$$

where $\partial A_{l,m}(t)/\partial t = a_{l,m}(t)$ and

$$N_{lmij} = \iint Y_{l,m}(\theta, \phi) Y_{i,j}(\theta, \phi) \cos\left(\frac{\omega}{c} |\mathbf{r} - \mathbf{r}'|\right) Y_{l,m}(\theta', \phi') Y_{i,j}(\theta', \phi') d\Omega' d\Omega, \quad (12)$$

where ω is the plasmon oscillation frequency. The potential energy $V_{l,m}$ of the l, m mode given by (11) is the same obtained by standard PHT, except for the inclusion of the factor N_{lmij} which, in the electrostatic limit, converges to $N_{lmij} = \delta_{li} \delta_{mj}$. Beyond the electrostatic limit, the overlap of the retarded plasmon modes with the Green's function expansion is no longer orthonormal and $\sum_{i,j} N_{lmij} < 1$. This reduces the Coulomb potential energy of the plasmon mode. Using (8) and (11) to define the Lagrangian $L_{l,m} = T_{l,m} - V_{l,m}$, and solving the Euler–Lagrange equations of motion [22], leads to the retarded plasmon frequency $\omega_{l,m}^{\text{sphere}}$ given by

$$\omega = \omega_{l,m}^{\text{sphere}} = \omega_B \sqrt{\frac{l}{2l+1}} R_{l,m}, \quad (13)$$

where

$$R_{l,m}^2 = \sum_{i,j} N_{lmij}.$$

Thus, for the simple case of a metallic nanosphere, the retarded plasmon frequency given by (13) is just the electrostatic frequency [13] scaled by a retardation factor $R_{l,m}$. However, for the case of more complex MNs with multiple plasmons that hybridize, the expression for the retarded plasmon frequency is more complex, as discussed in section 4 for a metallic nanotube.

It is important to note that (13) is an eigenequation, as the retardation factor $R_{l,m}$ is a function of $\omega_{l,m}^{\text{sphere}}$. To calculate $\omega_{l,m}^{\text{sphere}}$ by (13), one can solve this eigenequation with an iteration algorithm that we discuss in appendix A.

3.2. Comparison of retarded plasmon hybridization theory (RPHT) and Mie theory

We now use RPHT to calculate the retarded plasmon frequency of silver nanospheres in air and dielectric backgrounds. When dielectric inclusions are present, one needs to consider the bound surface charges at the metal–dielectric interfaces. These bound surface charges are induced by the plasmon modes via Coulomb interactions. By applying Maxwell's boundary conditions at the metal–dielectric interfaces, a relationship between the total surface charge distribution and the free surface charge distribution can be deduced [13].

In the case of a metallic nanosphere in a dielectric background of permittivity ϵ_D , the electrostatic plasmon frequency becomes red-shifted by a factor [13]

$$X = \sqrt{\frac{2l+1}{l + \epsilon_D(l+1)}}.$$

For plasmonic particles of finite size, these Coulomb interactions that induce the bound surface charges become retarded. Thus, the calculation of the bound surface charges are also

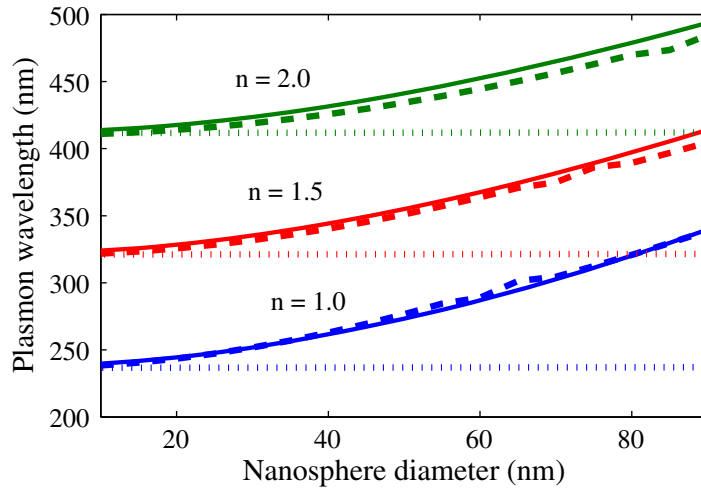


Figure 1. Comparison of Mie theory (solid) with RPHT (dashed) and electrostatic PHT (dotted) for a silver nanosphere embedded in a dielectric background of refractive index $n = 1.0$ (blue), $n = 1.5$ (red) and $n = 2.0$ (green).

affected by retardation. These higher-order retardation effects may become significant for very large plasmonic particles where magnetic interactions are also significant. For the purpose of this paper, we shall only consider the bound surface charge induced by the electrostatic fields. We will show by comparison with Mie theory that these assumptions are reasonable within the regime considered here.

Under these assumptions, the retarded plasmon frequency of a metallic nanosphere in dielectric background is given as

$$\omega_{l,m}^{\text{sphere}} = \sqrt{\frac{2l+1}{l+\epsilon_D(l+1)}} \omega_B \sqrt{\frac{l}{2l+1}} R_{l,m}. \quad (14)$$

To illustrate the accuracy of RPHT here, we give a comparison of RPHT with Mie theory [23], which is an exact solution to Maxwell's equations for spherical symmetry.

We assume Drude dielectric for silver with a bulk plasma frequency of $\omega_B = 1.37 \times 10^{16} \text{ rad s}^{-1}$ and a collision frequency of $\omega_c = 2.73 \times 10^{13} \text{ rad s}^{-1}$ and use published Mie scattering codes [23]. This simple spherical geometry has been chosen to clearly illustrate the effects of retardation on localized plasmons and validate the RPHT methodology introduced here. However, it is important to note that at ultraviolet and visible wavelengths the use of the Drude model is inaccurate.

Appendix A discusses the calculation of the retarded plasmon frequency given by (14) using an iterative method. The first four modes of the spherical Green's function ($Y_{0,0}$, $Y_{1,0}$, $Y_{1,1}$ and $Y_{1,-1}$) are used. The inclusion of higher-order modes has no significant effect on the results of RPHT in this regime. Figure 1 contains a plot of the fundamental ($l = 1$, $m = 0$) plasmon wavelength of a silver nanosphere for varying diameter using Mie theory (solid), RPHT (dashed) and electrostatic PHT (dotted). The nanosphere is embedded in a dielectric with refractive indices $n = 1.0$ (blue), $n = 1.5$ (red) and $n = 2.0$ (green). We observe excellent agreement between Mie theory and RPHT over all diameters considered. For very small diameters we see that both Mie theory and RPHT converge to the electrostatic PHT, where retardation is negligible and $R_{l,m} = 1$. At larger diameters (D), where $D > \lambda/10$, retardation weakens the

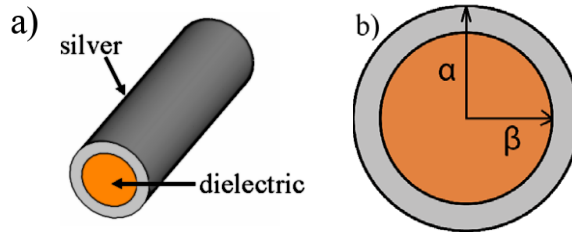


Figure 2. (a) Metallic (silver) nanotube with a dielectric core. (b) Cross-section of a metallic nanotube.

Coulomb interaction, causing red-shifting of plasmon wavelengths away from the electrostatic limit. This was investigated previously [16] using Mie scattering theory for nanospheres and spherical nanoshells.

Without the presence of a dielectric background, i.e. $n = 1.0$, Mie theory and RPHT overlap perfectly to within numerical error. We see up to a 40% red-shift in the fundamental plasmon wavelength at a nanosphere diameter of 90 nm, where $D/\lambda \approx 1/4$. For the case of dielectric backgrounds with $n = 1.5$ and 2.0 there are small deviations between Mie theory and RPHT at large diameters. This could perhaps be due to the induced bound charge being affected by retardation or magnetic interactions, both of which are not considered here. However, the excellent agreement between Mie theory and RPHT for even a dielectric background suggests that retardation does not affect the dielectric scaling (X) significantly.

4. Nanotube

Here we use RPHT to investigate retarded plasmons of a metallic nanotube with a dielectric core of permittivity ϵ_C . This geometry is of interest, especially within the photonic crystal community, where metallic photonic crystals are built from dielectric rods uniformly coated with metals such as gold and silver [24]. These metallic structures may possess plasmons at the wavelengths of operation of the photonic crystal depending on the geometry of the structure. As these structures typically have rod sizes $D > \lambda/10$, retardation will be significant.

In [25], plasmon hybridization within hollow metallic nanotubes was investigated; however, retardation effects were not considered. To derive the retarded plasmon frequency for a metallic nanotube, we assume that the nanotubes are much longer than their cross-sectional diameters so they can be considered as infinitely long. Here plasmons will be localized in two dimensions (2D), so the RPHT system reduces to 2D. There are two types of plasmon to consider: stationary plasmons with constant phase along the rod and propagating plasmons with oscillating phase with wave vector, \mathbf{k} along the rod axis.

Here we consider a dielectric rod of radius β , surrounded by a metallic nanotube of outer radius α , as shown in figure 2.

4.1. Stationary retarded plasmons

For the case of stationary plasmons, the modes do not have varying phase along the axis of the nanotube. The 2D flow potential in polar co-ordinates is given by

$$\eta(r, \theta, t) = \sum_n [a_n(t)r^n + b_n(t)r^{-n}] \cos(n\theta), \quad (15)$$

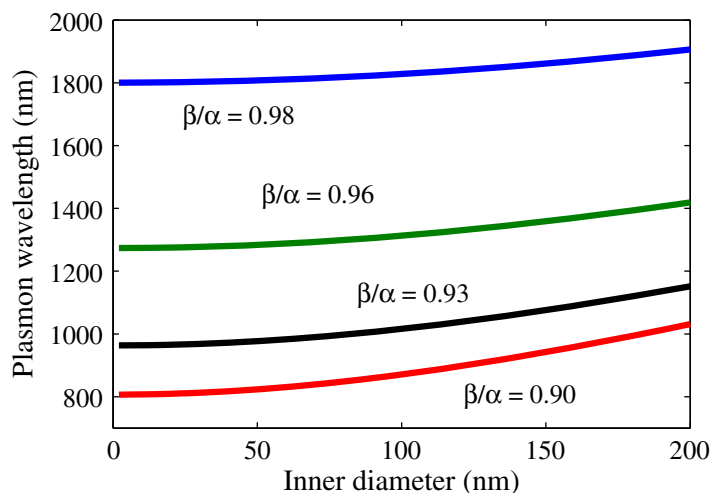


Figure 3. Plasmon hybridization and retardation within a silver nanotube with dielectric core of varying diameter. The ratios of inner/outer radii are $\beta/\alpha = 0.9$ (red), $\beta/\alpha = 0.93$ (black), $\beta/\alpha = 0.96$ (green) and $\beta/\alpha = 0.98$ (blue).

where $a_n(t)$ and $b_n(t)$ are the amplitudes of the n th outer and inner surface modes, respectively. The derivation of the kinetic energy T_n , and Coulomb potential energy V_n of the stationary retarded plasmon is given in appendix B. As seen for the retarded nanosphere, retardation factors appear in the potential energy for the nanotube. However, it is important to note that for the nanotube, retardation factors are different for each interaction, i.e. the inner–inner, outer–outer and inner–outer plasmon interactions have different degrees of retardation (see appendix B). Therefore, the effects of retardation on the plasmons are dependent on both the size and shape of the MN.

The eigenmodes of the system can be solved by diagonalization of the 2D Lagrangian $L_n = T_n - V_n$. This leads to a quadratic equation for the plasmon frequency, with two solutions corresponding to symmetric (low-frequency) and anti-symmetric (high-frequency) coupling between inner and outer surface plasmons. Here, we model the symmetric dipole ($n = 1$) stationary retarded plasmon. Again, we use the numerical iterative method to calculate the eigenfrequencies of RPHT. The nanotube consists of a silver nanotube surrounding a rod of Ormocer with $\epsilon_c = 2.43$ [26].

In figure 3, we plot the plasmon wavelength with the varying rod diameter for different ratios of inner/outer radii, β/α . The stationary plasmon wavelength of the silver nanotube depends on the shape of the MN (i.e. the ratio β/α), the size (retardation) and the dielectric constant of the rod. As $\beta/\alpha \rightarrow 1$, the nanotube thickness decreases, causing the hybridization between inner and outer plasmons to increase, which for the symmetric mode considered here, causes a strong red-shift in plasmon wavelengths. These plasmon hybridization effects are observed with electrostatic PHT in metallic spherical nanoshells [13]. For small rod diameters, we see that the plasmon wavelength is approximately independent of the diameter of the rod, which is the electrostatic regime where retardation is negligible.

However, unlike electrostatic PHT, here we see that for larger rod diameters there is significant retardation, which causes a further red-shifting to plasmon wavelengths. For the case of $\beta/\alpha = 0.9$, retardation causes a red-shifting of up to $\sim 20\%$ at a core diameter of 200 nm.

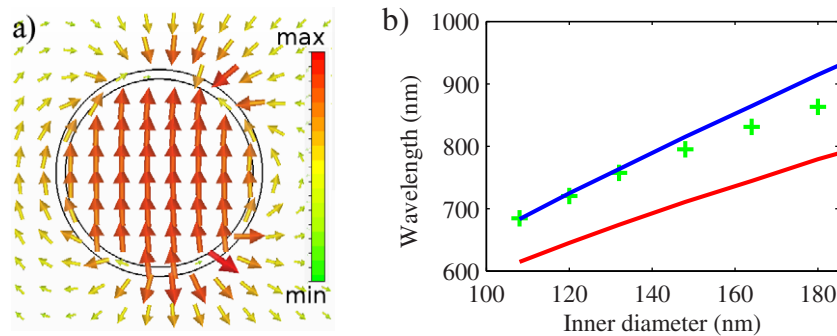


Figure 4. Fundamental symmetric plasmon wavelength of a hollow silver nanotube with a fixed shell thickness of 6 nm. (a) Electric field distribution of the plasmon resonance for a core diameter of 120 nm calculated via FIT. (b) Comparison of RPHT (blue), electrostatic PHT (red) and FIT (green crosses) for the varying core diameter.

For larger β/α (thinner nanotubes) hybridization red-shifts plasmons towards the electrostatic regime (longer wavelengths), where retardation is less significant.

We now compare electrostatic PHT, RPHT and numerical finite integration technique (FIT) using commercially available software, CST Microwave studio. FIT simulations are carried out in time domain and use the Drude parameters, as described above. In figure 4, we model the fundamental symmetric plasmon wavelength of a hollow silver nanotube with a fixed shell thickness of 6 nm. Figure 4(a) contains a vector plot of the plasmon electric field distribution calculated using the FIT for a core diameter of 120 nm. The field is incident from the left of the nanotube. The asymmetry of the electric field distribution about the vertical axis illustrates the de-phasing of the electric fields due to retardation.

Figure 4(b) contains a comparison of the plasmon wavelength calculated with electrostatic PHT, RPHT and FIT for varying core diameter. As the inner diameter of the nanotube increases, the hybridization between inner and outer surfaces becomes strong, causing red-shifting of the plasmon mode, as seen in all three models. For the parameters considered here the nanotube is in the retarded regime, and thus we see a significant red-shifting of the plasmon mode from its electrostatic limit shown in red. We see good agreement between the RPHT and FIT for the parameters considered here, showing the increased accuracy achieved through consideration of retardation effects. At larger nanotube diameters, where retardation becomes even greater, the RPHT and FIT have small differences in calculating the plasmon wavelength. Differences observed between the FIT and RPHT could be due to the lack of consideration in magnetic interactions, which become significant for highly retarded structures.

4.2. Propagating retarded plasmons

We now consider propagating plasmons of the form $\eta'(\mathbf{r}, t) = \eta(r, \theta, t)e^{ikz}$ where $k \neq 0$. The 2D flow potential of the n th mode is given by

$$\eta(r, \theta, t) = [a_n(t)I_n(kr) + b_n(t)K_n(kr)] \cos(n\theta), \quad (16)$$

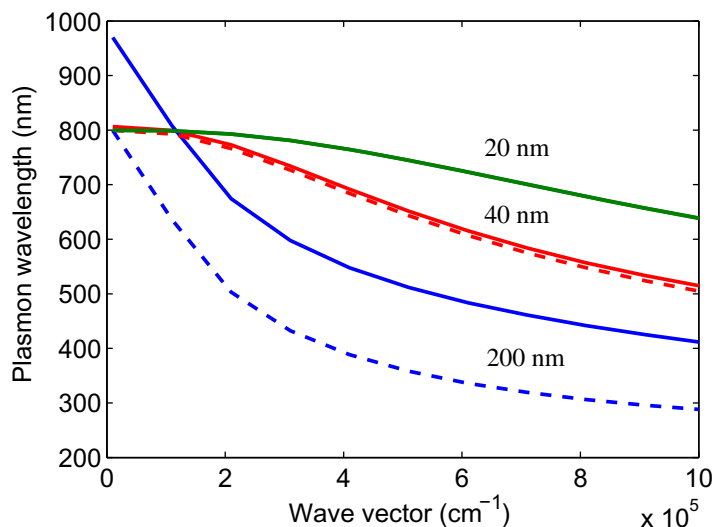


Figure 5. Dispersion of propagating, symmetric dipole plasmons calculated using RPHT (solid) and electrostatic PHT (dashed) for a silver nanotube with dielectric core diameters 20 nm (green), 40 nm (red) and 200 nm (blue). The dashed and solid green curves are overlapping.

where I_n and K_n are n th-order real modified Bessel functions. The derivation of the kinetic energy T_n , and Coulomb potential energy V_n of the propagating retarded plasmon is given in appendix C. As with the stationary case, the eigenmodes of the system can be solved by diagonalization of the 2D Lagrangian $L_n = T_n - V_n$.

We now model the symmetric dipole ($n = 1$) propagating retarded plasmon of the metallic nanotube. In figure 5, we plot the plasmon dispersion for a range of core diameters using both the electrostatic PHT (top) and RPHT (bottom). The ratio of inner/outer radii is fixed at $\beta/\alpha = 0.9$. As with the stationary case, the propagating plasmon wavelength of the silver depends on the shape of the MN, the size and the dielectric constant of the rod. However, for propagating plasmons there is the added dependence of the wave vector k of the propagating plasmon.

For both the RPHT and electrostatic PHT, the plasmon dispersion is increased as the core diameter is increased from 20 to 200 nm. The 20 and 40 nm nanotubes are much smaller than the wavelength of light and thus little difference is seen between the RPHT and PHT. However, when the size of the nanotube is increased to 200 nm retardation becomes significant. As observed for the stationary plasmon, where $k = 0$, retardation causes a red-shift of approximately 20%. As the plasmon wave vector increases, the plasmon wavelength decreases, causing retardation to become even stronger. For $k = 10^6 \text{ cm}^{-1}$ a red-shift of over 40% is seen. Thus, retardation causes a change in the dispersion characteristics of these metallic nanotubes.

5. Conclusion

PHT is an alternative model that can be used to investigate the coupling between plasmons within complex MNs. This method gives more insight into plasmon mechanics than is

achievable with direct solutions of Maxwell's equations. However, PHT is based on the electrostatic limit where MNs are much smaller than the wavelength of light.

We have extended the electrostatic PHT to include retardation effects to allow more accurate modeling of plasmons beyond the electrostatic limit. The RPHT developed here agrees well with Mie scattering theory for metallic nanospheres in both the electrostatic and retarded regimes, illustrating the accuracy of RPHT in both these regimes.

We have observed that retardation effects cause red-shifts in the plasmon wavelength, creating an extra degree of freedom in designing plasmonic nanostructures. We have used the RPHT to investigate the retarded plasmon modes in metallic nanotubes with dielectric cores. These plasmon modes are comparable to those observed recently within metallic photonic crystals [24]. We have shown that retardation can also alter the dispersion characteristics of propagating plasmons within metallic nanotubes.

In future work, more complex structures such as nanoparticle dimers or adjacent nanotubes might be considered. Further investigations on the effects of damping (loss) and magnetic interactions may also be of interest.

Acknowledgments

This work was produced with the assistance of the Australian Research Council (ARC) under the Centres of Excellence program. CUDOS (the Centre for Ultrahigh-bandwidth Devices for Optical Systems) is an ARC Centre of Excellence. MDT acknowledges the Australian postgraduate award and CRC for Polymers for funding.

Appendix A. Iterative method for RPHT

To solve the plasmon frequency with RPHT, one must solve an equation of the form $\omega = F(\omega)$, where $F(\omega)$ is given by the diagonalization of the Lagrangian of the retarded plasmon. To solve this equation, we start by calculating the electrostatic plasmon frequency (ω_0) given by electrostatic PHT. This estimate of the retarded plasmon frequency can then be used to calculate the retarded plasmon frequency via RPHT. By re-substituting the plasmon frequency with a weighted average given by

$$\omega_{i+1} = 0.2F(\omega_{i-1}) + 0.8F(\omega_i),$$

where the coefficients 0.2 and 0.8 were found to achieve good convergence for most parameters considered here. In the limit of infinite iterations, the solution will converge to the exact value. However, in practice one can iterate the system until a specific degree of accuracy is achieved. Convergence accuracies for calculations presented in this paper are typically 0.5% of the plasmon frequency. An example of the convergence of the RPHT is given in figure A.1, where we model the fundamental plasmon wavelength for a silver nanosphere of diameter 100 nm in a background material of $\epsilon_D = 2.43$. As the number of iterations increases, we see that the plasmon wavelength converges successfully.

This simple iteration method works for most parameters; however, for extremely large sizes convergence may not be successful and more complicated algorithms are required.

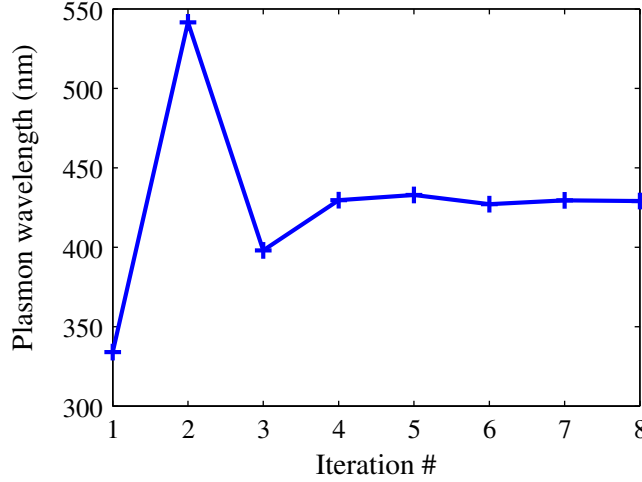


Figure A.1. Convergence of the RPHT by an iteration method.

Appendix B. Stationary nanotube plasmons

Here we derive the kinetic energy T_n and Coulomb potential energy V_n of the stationary-retarded plasmon. Using (15) in (1) gives the kinetic energy T_n as

$$T_n = \frac{n_0 m_e \pi n}{2} \begin{bmatrix} a_n \\ b_n \end{bmatrix}^T \begin{bmatrix} T_n^{11} & 0 \\ 0 & T_n^{22} \end{bmatrix} \begin{bmatrix} a_n \\ b_n \end{bmatrix}, \quad (\text{B.1})$$

where

$$T_n^{11} = [\alpha^{2n} - \beta^{2n}]$$

and

$$T_n^{22} = [\beta^{-2n} - \alpha^{-2n}].$$

The Coulomb potential of the system can be solved by using a polar Green's function expansion given by [21]

$$\frac{1}{|\mathbf{r} - \mathbf{r}'|} = 2 \sum_{m=1}^{\infty} \frac{1}{m} \left(\frac{r_{<}}{r_{>}} \right)^m \cos [m(\theta - \theta')], \quad (\text{B.2})$$

where $r_{>} = \max(r, r')$ and $r_{<} = \min(r, r')$. To calculate the Coulomb potential energy, we must first calculate the induced bound surface charge at the metal–dielectric interface. As in section 3, we use the electrostatic Coulomb potential to calculate this dielectric scaling of the surface charge distribution. The total surface charge σ_{inner}^t and σ_{outer}^t at the inner and outer surfaces, respectively, are related to the spill-out plasmon charge σ_{inner} and σ_{outer} by

$$\begin{bmatrix} \sigma_{\text{inner}}^t \\ \sigma_{\text{outer}}^t \end{bmatrix} = \hat{X} \begin{bmatrix} \sigma_{\text{inner}} \\ \sigma_{\text{outer}} \end{bmatrix},$$

where \hat{X} is a 2×2 matrix that can be calculated through the boundary conditions

$$\sigma_{\text{outer,inner}} = \frac{1}{4\pi} \left[\epsilon_C \frac{\partial \Phi}{\partial r} - \epsilon_M \frac{\partial \Phi}{\partial r} \right]_{r=\alpha,\beta} \quad (\text{B.3})$$

and

$$\phi(r, \theta, t) = \int \frac{\sigma_{\text{inner}}^t(\theta', t)}{|\mathbf{r} - \mathbf{r}'|} dS' + \int \frac{\sigma_{\text{outer}}^t(\theta', t)}{|\mathbf{r} - \mathbf{r}'|} dS'. \quad (\text{B.4})$$

Solving (B.3) gives the dielectric scaling matrix \hat{X} as

$$X = \begin{bmatrix} \Gamma_1 & -\Gamma_2 \alpha / \beta \\ 0 & 1 \end{bmatrix}, \quad (\text{B.5})$$

where

$$\Gamma_1 = \frac{2}{(\epsilon_C + 1)}$$

and

$$\Gamma_2 = \left(\frac{\beta}{\alpha}\right)^n \frac{(\epsilon_C - 1)}{(1 + \epsilon_C)}.$$

Equation (B.5) tells us that the total inner surface charge distribution is affected by the dielectric presence and has contributions from both the inner and outer surface plasmons. For a hollow core, i.e. $\epsilon_C = 1$, X reduces to the identity matrix as expected. The retarded potential energy of the system can then be calculated via [13]

$$V = \frac{1}{2} \int \sigma_{\text{outer}}^t(\theta, t) \tilde{\phi}(r = \alpha, \theta, t) \alpha d\theta + \frac{1}{2} \int \sigma_{\text{inner}}^t(\theta, t) \tilde{\phi}(r = \beta, \theta, t) \beta d\theta,$$

where $\tilde{\phi}(r, \theta, t)$ is the retarded Coulomb potential in the absence of a dielectric core, which can be calculated using (15) and (B.2) in (4). The Coulomb potential energy becomes

$$V_n = \pi^2 n_o^2 e^2 n \begin{bmatrix} A_n \\ B_n \end{bmatrix}^T \begin{bmatrix} V_n^{11} & V_n^{12} \\ V_n^{21} & V_n^{22} \end{bmatrix} \begin{bmatrix} A_n \\ B_n \end{bmatrix}, \quad (\text{B.6})$$

where

$$V_n^{11} = \sum_m \alpha^{2n} R_n^{\text{out}} + \beta^{2n} R_n^{\text{in}} \Gamma_1 - (1 + \Gamma_1) \beta^{2n} R_n^{\text{inout}} + \Gamma_2 \alpha^n \beta^n (R_n^{\text{in}} - R_n^{\text{inout}}),$$

$$V_n^{12} = V_n^{21} = \sum_m -R_n^{\text{out}} - \Gamma_1 R_n^{\text{in}} + \frac{(1 + \Gamma_1)}{2} R_n^{\text{inout}} + \frac{(1 + \Gamma_1)}{2} \frac{\beta^{2n}}{\alpha^{2n}} R_n^{\text{inout}} \\ - \frac{\Gamma_2}{2} R_n^{\text{in}} \left(\left(\frac{\alpha}{\beta}\right)^n + \left(\frac{\beta}{\alpha}\right)^n \right) + \Gamma_2 \left(\frac{\beta}{\alpha}\right)^n R_n^{\text{inout}},$$

$$V_n^{22} = \sum_m \alpha^{-2n} R_n^{\text{out}} + \Gamma_1 \beta^{-2n} R_n^{\text{in}} - \left(1 + \Gamma_1 + \Gamma_2 \frac{\beta^n}{\alpha^n}\right) \alpha^{-2n} R_n^{\text{inout}} + \Gamma_2 \beta^{-n} \alpha^{-n} R_n^{\text{in}}.$$

The retardation factors of the inner, outer and cross-coupling Coulomb interactions are given by R_{nm}^{in} , R_{nm}^{out} and R_{nm}^{inout} , respectively. These are given by the following integrals:

$$R_{nm}^{\text{out}} = \frac{1}{\pi^2} \iint \cos\left(\frac{\omega}{c} \alpha \sqrt{2} \sqrt{1 - \cos(\theta - \theta')}\right) \cos[m(\theta - \theta')] \cos(n\theta') d\theta' \cos(n\theta) d\theta,$$

$$R_{nm}^{\text{in}} = \frac{1}{\pi^2} \iint \cos\left(\frac{\omega}{c} \beta \sqrt{2} \sqrt{1 - \cos(\theta - \theta')}\right) \cos[m(\theta - \theta')] \cos(n\theta') d\theta' \cos(n\theta) d\theta$$

and

$$R_{nm}^{\text{inout}} = \frac{1}{\pi^2} \iint \cos\left(\frac{\omega}{c} \sqrt{\alpha^2 + \beta^2 - 2\alpha\beta \cos(\theta - \theta')}\right) \cos[m(\theta - \theta')] \cos(n\theta') d\theta' \cos(n\theta) d\theta,$$

where ω is the plasmon oscillation frequency.

The V_n^{11} and V_n^{22} terms represent the self-interaction of outer and inner surface plasmons, respectively, whereas the V_n^{12} and V_n^{21} terms represent the mutual interactions between inner and outer surface plasmons and indicate the strength of the plasmon hybridization [13].

Appendix C. Propagating nanotube plasmons

Here we derive the kinetic energy T_n and Coulomb potential energy V_n of the propagating retarded plasmon. Using (16) in (1) gives the kinetic energy as

$$T_n = \frac{n_o m_e \pi k}{2} \begin{bmatrix} a_n \\ b_n \end{bmatrix}^T \begin{bmatrix} T_n^{11} & T_n^{12} \\ T_n^{21} & T_n^{22} \end{bmatrix} \begin{bmatrix} a_n \\ b_n \end{bmatrix}, \quad (\text{C.1})$$

where

$$\begin{aligned} T_{11} &= I_n(k\alpha) I_n'(k\alpha) \alpha - I_n(k\beta) I_n'(k\beta) \beta, \\ 2T_{12} &= 2T_{21} = K_n(k\alpha) I_n'(k\alpha) \alpha + I_n(k\alpha) K_n'(k\alpha) \alpha \\ &\quad - I_n(k\beta) K_n'(k\beta) \beta - K_n(k\beta) I_n'(k\beta) \beta \end{aligned}$$

and

$$T_{22} = K_n(k\alpha) K_n'(k\alpha) \alpha - K_n(k\beta) K_n'(k\beta) \beta.$$

We shall now use a cylindrical expansion for Green's function given by [21]

$$\frac{1}{|\mathbf{r} - \mathbf{r}'|} = 4 \sum_{m=1}^{\infty} I_m(kr_<) K_m(kr_>) \cos(m(\theta - \theta')).$$

As for the stationary case, the dielectric scaling matrix can be calculated solving (B.3), which gives

$$\begin{bmatrix} \sigma_{\text{inner}}^t \\ \sigma_{\text{outer}}^t \end{bmatrix} = \begin{bmatrix} (\Gamma_1)^{-1} & \Gamma_2 \\ 0 & 1 \end{bmatrix} \begin{bmatrix} \sigma_{\text{inner}} \\ \sigma_{\text{outer}} \end{bmatrix},$$

where

$$\Gamma_1 = \epsilon_c k \beta I_n'(k\beta) K_n(k\beta) - k \beta I_n(k\beta) K_n'(k\beta) \quad (\text{C.2})$$

and

$$\Gamma_2 = - \frac{(\epsilon_c k \alpha I_n'(k\beta) K_n(k\alpha) - k \alpha I_n'(k\beta) K_n(k\alpha))}{(\epsilon_c k \beta I_n'(k\beta) K_n(k\beta) - k \beta I_n(k\beta) K_n'(k\beta))}. \quad (\text{C.3})$$

The retarded Coulomb potential energy then becomes

$$V_n = 2\pi^2 n_o^2 e^2 k^2 \begin{bmatrix} A_n \\ B_n \end{bmatrix}^T \begin{bmatrix} V_n^{11} & V_n^{12} \\ V_n^{21} & V_n^{22} \end{bmatrix} \begin{bmatrix} A_n \\ B_n \end{bmatrix}, \quad (\text{C.4})$$

where

$$V_n^{11} = \sum_{m=1}^{\infty} \alpha^2 (I'_n(k\alpha))^2 I_m(k\alpha) K_m(k\alpha) R_{nm}^{\text{out}} - \alpha\beta I'_n(k\alpha) I'_n(k\beta) K_m(k\alpha) I_m(k\beta) R_{nm}^{\text{inout}} \\ + \beta\alpha I'_n(k\alpha) K_m(k\alpha) I_m(k\beta) \{ \Gamma_2 I'_n(k\alpha) - \Gamma_1 I'_n(k\beta) \} R_{nm}^{\text{inout}} \\ + \beta^2 I'_n(k\beta) K_m(k\beta) I_m(k\beta) \{ \Gamma_1 I'_n(k\beta) - \Gamma_2 I'_n(k\beta) \} R_{nm}^{\text{in}},$$

$$V_n^{12} = \sum_{m=1}^{\infty} \alpha^2 I'_n(k\alpha) K'_n(k\alpha) K_m(k\alpha) I_m(k\alpha) R_{nm}^{\text{out}} - \frac{1}{2} \alpha\beta I'_n(k\alpha) K'_n(k\beta) K_m(k\alpha) I_m(k\beta) R_{nm}^{\text{inout}} \\ - \frac{1}{2} \alpha\beta K'_n(k\alpha) I'_n(k\beta) K_m(k\alpha) I_m(k\beta) R_{nm}^{\text{inout}} + \Gamma_2 I_m(k\beta) \\ \times \left\{ \beta\alpha I'_n(k\alpha) K'_n(k\alpha) K_m(k\alpha) R_{nm}^{\text{inout}} - \frac{\beta^2}{2} K_m(k\beta) \{ I'_n(k\alpha) K'_n(k\beta) + K'_n(k\alpha) I'_n(k\beta) \} R_{nm}^{\text{in}} \right\} \\ + \Gamma_1 I_m(k\beta) \left\{ \beta^2 I'_n(k\beta) K'_n(k\beta) K_m(k\beta) R_{nm}^{\text{in}} - \frac{\beta\alpha}{2} K_m(k\alpha) \{ I'_n(k\beta) K'_n(k\alpha) \right. \\ \left. + K'_n(k\beta) I'_n(k\alpha) \} R_{nm}^{\text{inout}} \right\},$$

and

$$V_n^{22} = \sum_{m=1}^{\infty} K'_n(k\alpha) K_m(k\alpha) \left\{ \alpha^2 K'_n(k\alpha) I_m(k\alpha) R_{nm}^{\text{out}} - \alpha\beta K'_n(k\beta) I_m(k\beta) R_{nm}^{\text{inout}} \right\} \\ + \Gamma_1 \beta I_m(k\beta) K'_n(k\beta) \left\{ \beta K'_n(k\beta) K_m(k\beta) R_{nm}^{\text{in}} - \alpha K'_n(k\alpha) K_m(k\alpha) R_{nm}^{\text{inout}} \right\} \\ + \Gamma_2 \beta K'_n(k\alpha) I_m(k\beta) \left\{ \alpha K'_n(k\alpha) K_m(k\alpha) R_{nm}^{\text{inout}} - \beta K'_n(k\beta) K_m(k\beta) R_{nm}^{\text{in}} \right\}.$$

References

- [1] Rand B P, Peumans P and Forrest S R 2004 *J. Appl. Phys.* **96** 7519–26
- [2] Pillai S, Catchpole K R, Trupke T and Green M A 2007 *J. Appl. Phys.* **101** 3105
- [3] Catchpole K R and Polman A 2008 *Opt. Express* **16** 21793–800
- [4] Otto A, Mrozek I, Grabhorn H and Akemann W 1992 *J. Phys.: Condens. Matter* **4** 1143–212
- [5] Mock J J, Barbic M, Smith D R, Schultz D A and Schultz S 2002 *J. Chem. Phys.* **116** 6755–9
- [6] Maier S A and Atwater H A 2005 *J. Appl. Phys.* **98** 011101–10
- [7] Nikolajsen T, Leosson K and Bozhevolnyi S I 2004 *Appl. Phys. Lett.* **85** 5833–5
- [8] Fang N, Lee H, Sun C and Zhang X 2005 *Science* **308** 534–7
- [9] Pendry J B, Holden A J, Stewart W J and Youngs I 1996 *Phys. Rev. Lett.* **76** 4773
- [10] Pendry J, Holden A, Robbins D and Stewart W 1999 *IEEE Trans. Microw Theory* **47** 2075–84
- [11] Smith D R, Pendry J B and Wiltshire M C K 2004 *Science* **305** 788–92
- [12] Prodan E, Radloff C, Halas N J and Nordlander P 2003 *Science* **302** 419–22
- [13] Prodan E and Nordlander P 2004 *J. Chem. Phys.* **120** 5444–54
- [14] Mayergoyz I D, Fredkin D R and Zhang Z 2005 *Phys. Rev. B* **72** 155412
- [15] Davis T J, Vernon K C and Gomez D E 2009 *Phys. Rev. B* **79** 155423
- [16] Tam F, Chen A L, Kundu J, Wang H and Halas N J 2007 *J. Chem. Phys.* **127** 204703–6
- [17] Moreno E, Erni D, Hafner C and Vahldieck R 2002 *J. Opt. Soc. Am. A* **19** 101–11

- [18] Myroshnychenko V, Rodriguez-Fernandez J, Pastoriza-Santos I, Funston A M, Novo C, Mulvaney P, Liz-Marzan L M and de Abajo F J G 2008 *Chem. Soc. Rev.* **37** 1792–805
- [19] Nordlander P, Oubre C, Prodan E, Li K and Stockman M I 2004 *Nano Lett.* **4** 899–903
- [20] Wang H, Brandl D W, Le F, Nordlander P and Halas N J 2006 *Nano Lett.* **6** 827–32
- [21] Jackson J D 1998 *Classical Electrodynamics* 3rd edn (New York: Wiley)
- [22] Goldstein H, Poole C P and Safko J L 2002 *Classical Mechanics* 3rd edn (Reading, MA: Addison-Wesley)
- [23] Matzler C 2002 Matlab functions for Mie scattering and absorption *Technical Report* Institut für Angewandte Physik
- [24] Li J, Hossain M M, Jia B, Buso D and Gu M 2010 *Opt. Express* **18** 4491–8
- [25] Moradi A 2008 *J. Phys. Chem. Solids* **69** 2936–8
- [26] Li J, Jia B and Gu M 2008 *Opt. Express* **16** 20073–80